A Novel Beam Domain Channel Model for B5G Massive MIMO Wireless Communication Systems

Fan Lai, *Student Member, IEEE*, Cheng-Xiang Wang, *Fellow, IEEE*, Jie Huang, *Member, IEEE*, Xiqi Gao, *Fellow, IEEE*, and Fu-Chun Zheng, *Senior Member, IEEE*

***Abstract*—In this paper, a novel beam domain channel model (BDCM) is proposed for beyond fifth generation (B5G) massive multiple-input multiple-output (MIMO) wireless communication systems. Different from conventional massive MIMO BDCMs which assumed the far-field plane wavefront effect, the proposed BDCM considers more realistic spherical wavefront caused by near-field effect. We transform a massive MIMO geometry-based stochastic model (GBSM) from the antenna domain to the beam domain through specific algorithms to obtain the novel BDCM. The space-time-frequency correlations of both the GBSM and BDCM are studied, and the correlations for both models at the cluster level are similar. We also compare the quasi-stationary distance (QSD), computational complexity, and channel capacity for both models. Results show that in comparison to the GBSM, the novel BDCM has lower complexity and similar accuracy if the number of beams is sufficiently large. Furthermore, we compare the singular value spreads (SVSs) of both channel models with channel measurements under the same conditions. Both the novel BDCM and GBSM are close to the measurement. Through the above analysis, the novel BDCM is proved to be more convenient for information theory and signal processing researches than the conventional GBSMs.**

***Index Terms*—B5G, beam domain channel model, GBSM, massive MIMO, statistical properties.**

Manuscript received 6 December 2021; revised 3 July 2022 and 30 August 2022; accepted 2 November 2022. Date of publication 17 November 2022; date of current version 18 April 2023. This work was supported in part by the National Key R&D Program of China under Grant 2018YFB1801101, in part by the National Natural Science Foundation of China (NSFC) under Grants 61960206006, 61901109, and 62271147, in part by the Key Technologies R&D Program of Jiangsu (Prospective and Key Technologies for Industry) under Grants BE2022067 and BE2022067-1, in part by the Frontiers Science Center for Mobile Information Communication and Security, the Research Fund of the National Mobile Communications Research Laboratory, Southeast University under Grant 2021B02, in part by EU H2020 RISE TESTBED2 Project under Grant 872172, in part by High Level Innovation and Entrepreneurial Doctor Introduction Program in Jiangsu under Grant JSSCBS20210082, in part by the Fundamental Research Funds for the Central Universities under Grant 2242022R10067, and in part by Shenzhen Science and Technology Program under Grant KQTD20190929172545139. The review of this article was coordinated by Dr. Huiling Zhu. *(Corresponding authors: Cheng-Xiang Wang; Fu-Chun Zheng.)*

Fan Lai, Cheng-Xiang Wang, Jie Huang, and Xiqi Gao are with the National Mobile Communications Research Laboratory, School of Information Science and Engineering, Southeast University, Nanjing 210096, China, and also with the Purple Mountain Laboratories, Nanjing 211111, China (e-mail: lai_fan@seu.edu.cn; chxwang@seu.edu.cn; j_huang@seu.edu.cn; xqgao@seu.edu.cn).

Fu-Chun Zheng is with the School of Electronic and Information Engineering, Harbin Institute of Technology (Shenzhen), Shenzhen 518055, China, and also with the National Mobile Communications Research Laboratory, Southeast University, Nanjing 210096, China (e-mail: fzheng@ieee.org).

Digital Object Identifier 10.1109/TVT.2022.3222771

I. Introduction

NOWADAYS, the fifth generation (5G) [1] wireless communication network has gradually been deployed worldwide and beyond 5G (B5G) networks are expected to be developed over the next decade [2]. Compared with previous generations of wireless communication networks, B5G will significantly improve data rate, coverage, security, adaptability, and scalability [3]. Massive multiple-input multiple-output (MIMO) can greatly reduce the difficulty of signal processing [4], simplify the process, improve the system performance compared with traditional MIMO technologies, and has attracted extensive attention for 5G and B5G researchers [5]. Massive MIMO technology equips hundreds and thousands of antennas at the base station (BS) side, at least one order of magnitude more than the active terminal side, to utilize the asymptotic characteristics of some particular kinds of wireless channels [6].

So far, many works have been done for massive MIMO wireless communication systems, such as performance analysis, pilot contamination reduction, channel estimation, etc. Channel models are fundamentals for the research, analysis, and evaluation of massive MIMO wireless communication systems [7], as well as a key index to measure system performance [8]. Massive MIMO channel models are generally divided into deterministic channel models and stochastic channel models. In deterministic channel models, such as channel measurements and ray-tracing channel models, all model parameters are fixed. They are precise for site-specific scenarios but usually bring high complexity. Stochastic channel models consist of correlation-based stochastic model (CBSM) and geometry-based stochastic model (GBSM).

The complexities of GBSMs are much lower than that of deterministic channel models, and GBSMs are suitable for system-level simulations and performance analysis of massive MIMO systems. Multiple massive MIMO GBSMs in recent years have been reviewed in [9]. In [10], the authors proposed a two-dimensional (2D) non-stationary wideband ellipse channel model, where all scatterers are distributed on multiple con-focal ellipses. The proposed GBSM considered near-field spherical wavefront effect and spatial non-stationarity, which were observed by massive MIMO channel measurements [11], [12], [13]. Massive MIMO channel models based on multiple rings and double rings were proposed in [14] and [15], respectively. The non-stationarity over the array axis were modeled via the birth-death process of clusters. Spherical wavefront effect and parameter drifting on the array axis were modeled through geometric relations. In [16], the authors proposed a three-dimensional (3D) non-stationary wideband massive MIMO channel model, which innovatively abstracted the complex scattering environment by using a virtual link. An approximation algorithm for calculating spherical wavefront, namely parabolic wavefront, was introduced. The algorithm can linearly model the angular drift of large antenna array and greatly reduce the computational complexity of the model. In [17], the authors extended the parabolic wavefront model to 3D space-time domain. Another massive MIMO channel model based on the WINNER model was proposed in [18]. Different from [17], the non-stationarity over the array axis was modeled by dividing the BS antenna array into several sub-arrays. In [19] and [20], Gao et al. proposed a massive MIMO channel model based on the COST 2100 model [21]. The visible region (VR) was introduced to model the space non-stationarity. In [22], Xie et al. proposed a 3D cylindrical massive MIMO channel model, in which a 3D sphere VR was assigned to each antenna, to model the space non-stationarity. In addition, a 3D 5G general channel model was proposed in [23], which was applicable to a wide range of scenarios, including massive MIMO, millimeter-wave (mmWave), vehicle-to-vehicle (V2V), and high-speed train (HST) scenarios. In [29], the MIMO channel blockage model, path loss model, and time-varying channel model applicable to mmWave scenarios were proposed. A more general 3D B5G channel model was proposed in [24], which can be suitable for massive MIMO, V2V, HST, and mmWave-Terahertz (THz) communication scenarios. In [25], authors proposed a temporally non-stationary unmanned aerial vehicle (UAV)-to-ground channel model by introducing an aeronautic random mobility model (RMM) into a GBSM. Time-varying model parameters including delays and angles of multi-path components (MPCs) were derived in this model. A novel space-time-frequency non-stationary GBSM for ultra-massive MIMO THz channels considering long traveling paths is first proposed in [26]. Authors in [27] proposed a novel 3D non-stationary wideband massive MIMO channel model capturing the space-time ray-level evolution. In [28], a 6 G pervasive channel model (6GPCM) was proposed using a unified channel modeling method, with a GBSM framework considering all spectra from sub-6 GHz to visible light communication (VLC) bands, global-coverage scenarios, and full-application scenarios in the 6 G wireless communication systems.

However, the complexities of GBSMs mentioned above are still high, which are only suitable for system-level simulations and model validation, but not for information theory and signal processing research. At this point, simplified GBSMs or CBSMs will be promising. CBSMs can be divided into classical independent and identically distributed (i.i.d.) Rayleigh fading channel models and correlated channel models [9]. Correlated channel models can be divided into separate correlated channel models, i.e., Kronecker-based stochastic models (KBSMs) [30], and jointly correlated channel models including the Weichselberger model [31] and the virtual channel representation (VCR) model [32]. In [33] and [34], KBSMs were adopted which considered the correlation between antennas but the transmitter (Tx) and receiver (Rx) correlations were assumed to be independent of each other. KBSMs are easy to be implemented but the channel characteristics are somehow oversimplified. In [35], the authors adopted the Weichselberger model jointly considering the antenna correlations at both ends. This model is more realistic than KBSMs and has widely been used to analyze the performance of massive MIMO systems. The VCR model used discrete Fourier transform (DFT) matrices to model MIMO channels. Authors in [36] pointed out that with the increase of the number of antennas, the angular division of VCR model will become denser, the angular resolution will be improved, and the model accuracy will also be improved accordingly. The VCR model was studied from the perspective of channel capacity in [37]. However, the disadvantage of the VCR model is that it is only applicable to uniform linear arrays (ULAs) [32]. Recently, Dahiya [38] and Joung et al. [39] proposed several massive MIMO channel models based on CBSMs.

The above traditional CBSMs did not consider the spherical wavefront caused by the near-field effect and the spatial non-stationarity. They are not suitable for massive MIMO channel modeling research. Recently, in [40], the authors first proposed a beam domain channel model (BDCM) for massive MIMO scenarios by transforming the channel from the antenna domain to the beam domain via two unitary matrices, but still considered the far-field effect. This model has been widely used in various signal processing researches, especially beam division multiple access (BDMA) [40], [41], [42], [43]. However, like traditional CBSMs, they did not take the new features of massive MIMO channels into account. Therefore, a realistic channel model considering the near-field effect and spatial non-stationarity and with low complexity suitable for information theory and signal processing researches of massive MIMO systems is urgently needed.

The limitations of the VCR model in [32] is that it is not suitable for modeling channels with non-ULAs or massive MIMO antenna arrays. To solve this problem, a novel BDCM that can be considered as an extension to the VCR model in [32] is proposed in this paper. Different modeling methods of virtual angles are utilized and new characteristics of massive MIMO channels are introduced. We summarize the novelties and main contributions of this paper as follows:

1) A novel BDCM for B5G massive MIMO communication systems is proposed for the first time by transferring a conventional GBSM from the antenna domain to the beam domain and considers the near-field effect and non-stationarities of massive MIMO channels.
2) Statistical properties of both the GBSM and proposed BDCM, such as the space-time-frequency correlation function (STFCF) with its deductions and quasi-stationary distance (QSD) are studied and compared.
3) The impacts of the GBSM and BDCM on the system performance, e.g., channel capacities and singular value spread (SVSs), are also studied and compared.
4) Besides the above accuracy aspects, i.e., statistical and system properties, we have for the first time investigated and compared the computational complexities of both the GBSM and BDCM.

The remainder of this paper is organized as follows. Section II gives a brief introduction to an conventional non-stationary

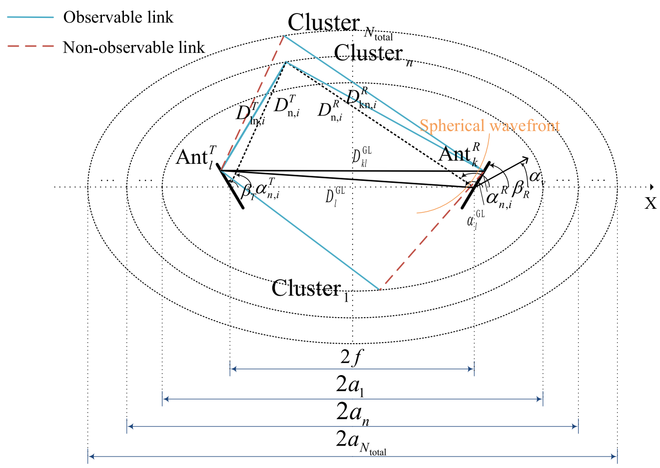

Fig. 1. Illustration of the conventional non-stationary wideband GBSM [10].

wideband GBSM. We propose a novel BDCM and it will be discussed in Section III. In Section IV, the analysis of statistical properties for both models is presented. Computational complexity and channel capacity analysis of both models are conducted in Section V. Section VI shows the results and discussions. In Section VII, we draw the conclusions.

II. A Conventional Non-Stationary Wideband GBSM

Let us begin with an conventional non-stationary wideband GBSM [10], as shown in Fig. 1. The numbers of Tx and Rx antennas are M_T and M_R. The antenna elements are spaced with separation δ_T and δ_R. They are located at the focal points of the confocal ellipses with a distance of $2f$. Let Ant_l^T represent the l-th antenna of the transmit array and Ant_k^R represent the k-th antenna of the receive array. The n-th cluster is on the n-th ellipse with major axis $2a_n$. The angle $\beta_T(\beta_R)$ denotes the tilt angle of the transmit (receive) antenna array. The angle α_v denotes the angle between the x-axis and the direction of movement of the receiver. The maximum Doppler frequency and carrier wavelength are denoted as $f_{\max}$ and λ, respectively. The total number of clusters which are observable to at least one Tx and Rx antenna, is denoted as N_{total}.

$$N_{\text{total}} = \text{card}\left(\bigcup_{l=1}^{M_T}\bigcup_{k=1}^{M_R}\left(C_l^T(t)\bigcap C_k^R(t)\right)\right) \tag{1}$$

The number of elements in the set is called the cardinality of the set, represented as $\text{card}(\cdot)$. C_l^T (C_k^R) denotes the cluster set in which clusters are observable to Ant_l^T (Ant_k^R). The n-th cluster is called Cluster_n. If and only if $\text{Cluster}_n \in \{C_l^T \bigcap C_k^R\}$, we can say $\text{Cluster}_n (n \leq N_{\text{total}})$ is observed by both Ant_l^T and Ant_k^R. The channel is modeled as an $M_R \times M_T$ matrix $\mathbf{H}_G(t,\tau) = [h_{kl}(t,\tau)]_{M_R\times M_T}$ with complex-valued elements

$$h_{kl}^G(t,\tau) = \sum_{n=1}^{N_{\text{total}}} h_{kl,n}^G(t)\delta(\tau-\tau_n) \tag{2}$$

where $k = 1,2,\ldots,M_R$ and $l = 1,2,\ldots,M_T$. The line-of-sight (LOS) component and non-line-of-sight (NLOS) components consist $h_{kl,n}^G(t)$. The delay of Cluster_n is denoted as τ_n. The mean power of the n-th cluster is assumed as P_n. The key parameter definitions of the conventional GBSM are summarized in Table I. Then, the channel was modeled as

—if $\text{Cluster}_n \in \{C_l^T \bigcap C_k^R\}$,

$$h_{kl,n}^G(t) = \underbrace{\delta(n-1)\sqrt{\frac{K}{K+1}}e^{j(2\pi f_{kl}^{\text{GL}}t+\varphi_{kl}^{\text{GL}})}}_{\text{LOS}} + \underbrace{\sqrt{\frac{P_n}{K+1}}\lim_{S\to\infty}\frac{1}{\sqrt{S}}\sum_{i=1}^{S}e^{j(2\pi f_{n,i}t+\varphi_{kl,n,i})}}_{\text{NLOS}} \tag{3}$$

—if $\text{Cluster}_n \notin \{C_l^T \bigcap C_k^R\}$,

$$h_{kl,n}^G(t) = 0. \tag{4}$$

where K is the Rician factor. Parameters f_{kl}^{GL} and φ_{kl}^{GL} denote the carrier frequency and phase for the LOS component between A_l^T and A_k^R, respectively. Similarly, $f_{n,i}$ and $\varphi_{kl,n,i}$ represent the carrier frequency and phase for the NLOS component between A_l^T and A_k^R via the i-th ray within Cluster_n $(i = 1,2,\ldots,S)$, respectively. The detailed calculations of parameters f_{kl}^{GL}, φ_{kl}^{GL}, $f_{n,i}$, and $\varphi_{kl,n,i}$ can be found in [10], and we will not go into details. The conventional GBSM modeled the space non-stationarity by using birth-death process on the array axis [10]. The clusters appeared and disappeared randomly over the antenna array. The model also incorporates the birth-death process on the time axis [45]. The geometry is changed over time. In addition, cluster sets of antennas also evolve over time and are modeled as a birth-death process.

III. A Novel BDCM

Due to the high complexity of the conventional GBSM, we propose a novel BDCM in this section, which is more suitable for the research on information theory and signal processing. The proposed model transfer the channel from the antenna domain to the beam domain. Table II summarizes key parameter definitions of the novel BDCM.

According to [32], the finite dimensions of the signal space can be linearly decomposed into virtual channel representations in different virtual directions, which is very similar to the beamspace and wavenumber domain in array signal processing. This means that instead of dividing the channel or signal space by different antenna pairs, which has always been used in GBSMs or physical models, a new idea can be adopted, which is to divide the channel or signal space by beams. BDCM is such kind of channel model, which divides the channel according to the direction of transmitting and receiving angles, and then models and superimposes each sub-channel.

As for the beam division method, literature [32] provides the method of dividing the beam according to the angle cosine value. However, due to the non-monotone of the cosine function on $(-\pi,\pi]$, the VCR model can only distinguish the beam of 180°. However, the actual electromagnetic wave emission exists in all directions, so this classification method has certain limitations. The method adopted in this paper is to divide the angles on

TABLE I
KEY PARAMETER DEFINITIONS OF THE EXISTING GBSM

Parameter	Definition
$\text{Ant}_l^T(\text{Ant}_k^R)$	Tx antenna l (Rx antenna k)
τ_n	The delay of the cluster n
$\delta_T(\delta_R)$	The Tx (Rx) antenna spacing
$\alpha_{n,i}^T(\alpha_{n,i}^R)$	AoD (AoA) of the cluster n via path i to the Tx (Rx) array center
$f_{n,i}$	The Doppler frequency of cluster n via the path i
$\varphi_{kl,n,i}$	The phase of cluster n between Tx antenna l and Rx antenna k via the path i
$D_{ln,i}^T(D_{kn,i}^R)$	The distance between Tx antenna l (Rx antenna k) and cluster n via the path i
$D_{n,i}^T(D_{n,i}^R)$	The distance between Tx (Rx) antenna center and cluster n via the path i
f_{kl}^{GL}	The LOS Doppler frequency from Tx antenna l to Rx antenna k for GBSM
φ_{kl}^{GL}	The phase of the LOS path from Tx antenna l to Rx antenna k for GBSM
α_l^{GL}	The LOS AoA from Tx antenna l to Rx antenna center for GBSM
D_{kl}^{GL}	The LOS distance from Tx antenna l to Rx antenna k for GBSM
D_l^{GL}	The LOS distance from Tx antenna l to Rx antenna center for GBSM
α_v	The angle of the MS velocity

TABLE II
KEY PARAMETER DEFINITIONS OF THE NOVEL MASSIVE MIMO BDCM

Parameter	Definition
θ_m	The virtual angle of the cluster m to the Rx array center
f_m	The Doppler frequency of cluster m
a_m	The semi-major axis of the cluster m
$\varphi_{kl,m,i}$	The phase of cluster m between Tx antenna l and Rx antenna k via the path i
$D_{lm,i}^T(D_{km,i}^R)$	The distance between Tx antenna l (Rx antenna k) and cluster m via the path i
$D_{m,i}^T(D_{m,i}^R)$	The distance between Tx (Rx) antenna center and cluster m via the path i
f_{kl}^{BL}	The LOS Doppler frequency from Tx antenna l to Rx antenna k for BDCM
φ_{kl}^{BL}	The phase of the LOS path from Tx antenna l to Rx antenna k for BDCM
α_l^{BL}	The LOS AoA from Tx antenna l to Rx antenna center for BDCM
D_{kl}^{BL}	The LOS distance from Tx antenna l to Rx antenna k for BDCM
D_l^{BL}	The LOS distance from Tx antenna l to Rx antenna center for BDCM

$(-\pi, \pi]$ directly, instead of using cosine values. This avoids the problem of beam resolution. The specific division method is as follows:

AoAs of the physical channel are sampled uniformly over the interval $(-\pi, \pi]$, and we achieve the virtual angles, θ_m denoted as

$$\theta_m = -\pi + \frac{2\pi m}{M}, \quad m = 1, \ldots, M \tag{5}$$

where m denotes the sampling index of the virtual angle, and M is the total sampling number. We assume M is finite, and one steering vector with a virtual angle represents a beam. The relationship between AoDs, ϕ_m and AoAs, θ_m is the same as the above-mentioned GBSM, and let $\phi_m = \kappa(\theta_m)$, where $\kappa(\cdot)$ denote the function transforming AoAs to AoDs described in [10].

A. The NLOS Condition

Illustration of the NLOS channel for the novel BDCM is shown in Fig. 2. The NLOS parameters are all dependent on the arrival angles, which are defined as

$$f_m = f_{\max} \cos(\theta_m - \alpha_v) \tag{6}$$

$$\varphi_{kl,m,i} = \varphi_0 + \frac{2\pi}{\lambda}\left[D_{lm,i}^T + D_{km,i}^R\right]$$

$$= \varphi_0 + \frac{2\pi}{\lambda}\Big[D_{m,i}^T + D_{m,i}^R - (D_{m,i}^T - D_{lm,i}^T) + (D_{km,i}^R - D_{m,i}^R)\Big] \tag{7}$$

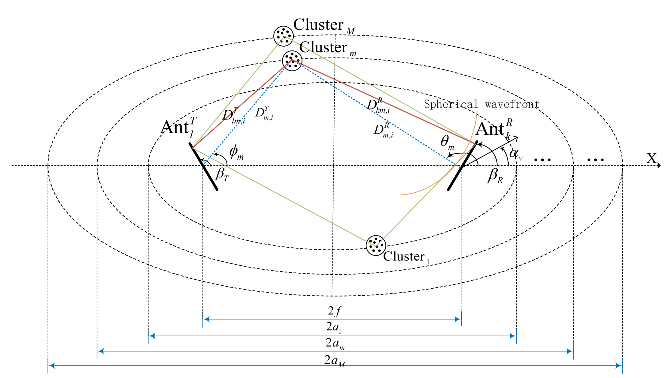

Fig. 2. Illustration of NLOS beam domain channel.

where

$$D_{m,i}^T = \frac{2a_m \sin\phi_{m,i}}{\sin\phi_{m,i} + \sin(\pi - \theta_{m,i})} \tag{8}$$

$$D_{m,i}^R = \frac{2a_m \sin(\pi - \theta_{m,i})}{\sin\phi_{m,i} + \sin(\pi - \theta_{m,i})}. \tag{9}$$

Here, the departure angles and the arrival angles of the paths within beam m are denoted as $\theta_{m,i}$ and $\phi_{m,i}$, which approximated as $\phi_{m,i} \approx \phi_m$ and $\theta_{m,i} \approx \theta_m$, respectively. Moreover, we have

$$D^T_{lm,i} = \left[(D^T_{m,i})^2 + \left(\frac{M_T - 2l + 1}{2}\delta_T\right)^2 - D^T_{m,i}(M_T - 2l + 1)\delta_T \cos(\beta_T - \phi_m)\right]^{1/2} \quad (10)$$

$$D^R_{km,i} = \left[(D^R_{m,i})^2 + \left(\frac{M_R - 2k + 1}{2}\delta_R\right)^2 - D^R_{m,i}(M_R - 2k + 1)\delta_R \cos(\theta_m - \beta_R)\right]^{1/2}. \quad (11)$$

B. The LOS Condition

The LOS parameters of the novel BDCM are defined as

$$f^{BL}_{kl} = f_{\max}\cos\left(\beta_R - \alpha_v + \arcsin\left[\frac{D^{\text{LOS}}_l}{D^{\text{LOS}}_{kl}} \times \sin\left(\alpha^{BL}_l - \beta_R\right)\right]\right) \quad (12)$$

$$\varphi^{\text{BL}}_{kl} = \varphi_0 + \frac{2\pi}{\lambda}D^{\text{BL}}_{kl} \quad (13)$$

where

$$D^{BL}_l = \left[(2f)^2 + \left(\frac{M_T - 2l + 1}{2}\delta_T\right)^2 - 2f(M_T - 2l + 1)\delta_T \cos\beta_T\right]^{1/2} \quad (14)$$

$$\alpha^{BL}_l = \arcsin\left[\frac{(M_T - 2l + 1)}{2D^{BL}_l}\sin\beta_T\right] \quad (15)$$

$$D^{BL}_{kl} = \left[(D^{BL}_l)^2 + \left(\frac{M_R - 2k + 1}{2}\delta_R\right)^2 - (M_R - 2k + 1)\delta_R D^{BL}_l \cos(\alpha^{BL}_l - \beta_R)\right]^{1/2}. \quad (16)$$

The LOS path can be also modeled by utilizing the NLOS paths with the same or similar arrival angles θ_{m_0}, which is depicted in Fig. 3. In this case, the AoD is $\phi_{m_0} = \kappa(\theta_{m_0})$, and we have the approximation as

$$\begin{aligned} D^{BL}_{kl} &\approx D^R_{km_0,i} - D^T_{lm_0,i},\ m_0 \in \mathcal{M} = \{1, 2, \ldots, M\} \\ &= D^R_{m_0,i} - D^T_{m_0,i} + (D^R_{km_0,i} - D^R_{m_0,i}) \\ &\quad + (D^T_{m_0,i} - D^T_{lm_0,i}). \end{aligned} \quad (17)$$

Based on the virtual angles, we model the steering vectors as

$$\mathbf{e}_T(\theta_m) = [e_T(1;\theta_m), \ldots, e_T(l;\theta_m), \ldots, e_T(M_T;\theta_m)]^T \quad (18)$$

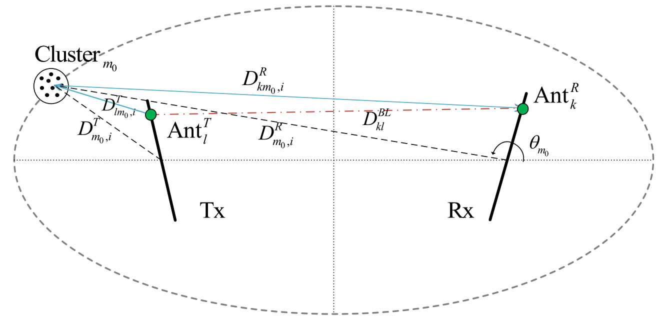

Fig. 3. Illustration of LOS beam domain channel.

$$\mathbf{e}_R(\theta_m) = [e_R(1;\theta_m), \ldots, e_R(k;\theta_m), \ldots, e_R(M_R;\theta_m)]^T \quad (19)$$

where

$$e_T(l;\theta_m) = e^{j\frac{2\pi}{\lambda}\left(D^T_{m,i} - D^T_{lm,i}\right)}, \quad l = 1, \ldots, M_T \quad (20)$$

$$e_R(k;\theta_m) = e^{j\frac{2\pi}{\lambda}\left(D^R_{km,i} - D^R_{m,i}\right)}, \quad k = 1, \ldots, M_R. \quad (21)$$

Thus, we have the theoretical model for the novel BDCM as

$$\begin{aligned} h^B_{kl,m}(t) = &\sqrt{\frac{K}{K+1}} e^{j\left[2\pi f^{\text{BL}}_{kl} t + \varphi_0 + \frac{2\pi}{\lambda}\left(D^R_{m_0,i} - D^T_{m_0,i}\right)\right]} \\ &\times e_R(k;\theta_{m_0}) \cdot e^*_T(l;\theta_{m_0}) + \lim_{M\to\infty}\sqrt{\frac{P_m}{(K+1)M}} \\ &\times \sum_{m=1}^{M} e^{j\left[2\pi f_m t + \varphi_0 + \frac{2\pi}{\lambda}\left(D^R_{m,i} + D^T_{m,i}\right)\right]} \\ &\times e_R(k;\theta_m) \cdot e^*_T(l;\theta_m). \end{aligned} \quad (22)$$

We define

$$\mathbf{H}_B(t) \triangleq \mathbf{U}_R\tilde{\mathbf{H}}_B(t)\mathbf{U}^H_T = \mathbf{U}_R\left[\tilde{\mathbf{H}}_{BL}(t) + \tilde{\mathbf{H}}_{BN}(t)\right]\mathbf{U}^H_T \quad (23)$$

where $\mathbf{U}_T \triangleq [\mathbf{e}_T(\theta_1), \ldots, \mathbf{e}_T(\theta_M)] \in \mathbb{C}^{M_T \times M}$, and $\mathbf{U}_R \triangleq [\mathbf{e}_R(\theta_1), \ldots, \mathbf{e}_R(\theta_M)] \in \mathbb{C}^{M_R \times M}$. We call $\tilde{\mathbf{H}}_B(t)$ as the beam domain channel matrix, where $\tilde{\mathbf{H}}_{BL}(t)$ and $\tilde{\mathbf{H}}_{BN}(t)$ means the LOS part and NLOS part, respectively.

$$[\tilde{\mathbf{H}}_{BL}(t)]_{m_0,m_0} = \delta(n-1)\sqrt{\frac{K}{K+1}} \times e^{j\left[2\pi f^{\text{BL}}_{kl} t + \varphi_0 + \frac{2\pi}{\lambda}\left(D^R_{m_0,i} - D^T_{m_0,i}\right)\right]} \quad (24)$$

$$[\tilde{\mathbf{H}}_{BN}(t)]_{m,m} = \sqrt{\frac{P_n}{(K+1)M}} \times e^{j\left[2\pi f_m t + \varphi_0 + \frac{2\pi}{\lambda}\left(D^R_{m,i} + D^T_{m,i}\right)\right]}. \quad (25)$$

When the number of beams is larger than the number of antennas, the channel can be accurately converted from the antenna domain to the beam domain. The larger the number of beams, the more accurate the channel model. When the number of beams tends to infinity, the accuracy of the proposed BDCM will tend to be the same as that of the conventional ellipse model. For practice, we only need to set the number of beams reasonably large to ensure the accuracy of the BDCM.

C. Relationship Between the Far-Field and Near-Field Assumptions

Traditional channel models is no longer valid. Thus, the spherical wave effect needs to be considered. Relationships between two assumptions will be discussed in this section. In massive MIMO channel models, the near-field effect is mainly reflected in the geometric relationships. Here, we investigate the distance values D_{lm}^T from Ant_l^T to $\mathrm{Cluster}_m$ and D_{km}^R from Ant_k^R to $\mathrm{Cluster}_m$. Under the near-field assumption, the values of them are represented as

$$D_{lm}^T = \Bigg[\left(D_m^T\right)^2 + \left(\frac{M_T - 2l + 1}{2}\delta_T\right)^2 - (M_T - 2l + 1)\delta_T D_m^T \cos(\beta_T - \phi_m)\Bigg]^{1/2} \tag{26}$$

$$D_{km}^R = \Bigg[\left(D_m^R\right)^2 + \left(\frac{M_R - 2k + 1}{2}\delta_R\right)^2 - (M_R - 2k + 1)\delta_R D_m^R \cos(\theta_m - \beta_R)\Bigg]^{1/2}. \tag{27}$$

If we ignore the large size of antennas and consider that the distance between antennas is much smaller than the distance between the transceiver and clusters, we will get the far-field assumption and degenerate to the plane wavefront model. The distance values are calculated as

$$D_{lm}^T = D_m^T - \left(\frac{M_T - 2l + 1}{2}\delta_T\right)\cos(\beta_T - \phi_m) \tag{28}$$

$$D_{km}^R = D_m^R - \left(\frac{M_R - 2k + 1}{2}\delta_R\right)\cos(\theta_m - \beta_R). \tag{29}$$

Note that under the far-field assumption with plane wavefront, the distance difference is linear with the antenna index difference. Thus, the corresponding steering vector is orthogonal. However, for the near-field case with spherical wavefront, the distance difference is non-linear with the antenna index difference and the corresponding steering vector becomes non-orthogonal.

According to Taylor series expansion formula, let $a = D_m^T$, $x = (M_T - 2l + 1)\delta_T/2, \gamma_T = \beta_T - \phi_m$ and then we plug this into (26) as

$$D_{lm}^T = \left(x^2 + a^2 - 2ax\cos\gamma_T\right)^{1/2} \triangleq g(x). \tag{30}$$

The derivative of $g(x)$ is

$$g'(x) = (x^2 + a^2 - 2ax\cos\gamma_T)^{-\frac{1}{2}}(x - a\cos\gamma_T). \tag{31}$$

We have the first-order Taylor series expansion of D_{lm}^T when x equals 0 as

$$\begin{aligned} D_{lm}^T &= g(x) \approx a - x\cos\gamma_T \\ &= D_m^T - \left(\frac{M_T - 2l + 1}{2}\delta_T\right)\cos(\beta_T - \phi_m). \end{aligned} \tag{32}$$

Similarly, D_{km}^R during the first-order Taylor series expansion can be derived as

$$D_{km}^R \approx D_m^R - \left(\frac{M_R - 2k + 1}{2}\delta_R\right)\cos(\theta_m - \beta_R). \tag{33}$$

According to the above derivation, we find the plane wavefront assumption is the first-order Taylor series expansion of the spherical wavefront and also a kind of approximation.

Furthermore, we do the the second-order Taylor series expansion of the spherical wavefront components, the second-order derivative of $g(x)$ is

$$\begin{aligned} g''(x) &= (x^2 + a^2 - 2ax\cos\gamma_T)^{-1/2} \\ &\quad - (x - a\cos\gamma_T)^2(x^2 + a^2 - 2ax\cos\gamma_T)^{-3/2}. \end{aligned} \tag{34}$$

Similar to the first-order, the second-order Taylor series expansions at $x_0 = 0$ are

$$\begin{aligned} D_{lm}^T &= g(x) \approx a - x\cos\gamma_T + x^2\frac{\sin^2\gamma_T}{2a} \\ &= D_m^T - \left(\frac{M_T - 2l + 1}{2}\delta_T\right)\cos(\beta_T - \phi_m) \\ &\quad + \frac{M_T - 2l + 1}{4}\delta_T\sin^2(\beta_T - \phi_m) \end{aligned} \tag{35}$$

$$\begin{aligned} D_{km}^R &\approx D_m^R - \left(\frac{M_R - 2k + 1}{2}\delta_R\right)\cos(\theta_m - \beta_R) \\ &\quad + \frac{M_R - 2k + 1}{4}\delta_R\sin^2(\theta_m - \beta_R) \end{aligned} \tag{36}$$

which are the parabolic wavefront assumption [17]. It is obvious that the parabolic wavefront assumption is another kind of approximation, which is more accurate than the plane wavefront.

IV. Statistical Property Analysis

In this section, the derivation of space-time-frequency correlation function (STFCF), space cross-correlation function (CCF), time auto-correlation function (ACF), and frequency correlation function (FCF) of GBSM and BDCM are given.

The STFCF calculates the correlation for channel gain between different antenna pairs. The space CCF, time ACF, and FCF (also known as frequency ACF) are the deductions of STFCF. They denote the space, time, and frequency correlations, respectively. Among them, the space CCF reflects the relevant characteristics of the channel in the space domain. Since massive MIMO antenna arrays are different from traditional smaller antenna arrays, the correlations between antennas are very important characteristics to be investigated directly. The time ACF reflects the correlation characteristics of the channel in the time domain. Considering the mobility of the transceiver and scatterer, both GBSM and BDCM need to consider the non-stationarity of the channel in the time domain. Such non-stationarity can be observed by the change trend of the time ACF at different moments. The FCF reflects the correlation of the channel in the frequency domain. By calculating the FCF, we can observe whether the correlation characteristics of both models are consistent in the frequency domain. In addition, we can obtain important channel parameters such as the correlation frequency.

A. Statistical Properties of the Conventional GBSM

Here, the statistical properties of the conventional GBSM will be briefly illustrated because authors of [10] have already studied them.

1) The Space CCF: In the antenna domain, the normalized space CCF $\rho^G_{kl,k'l,'n}(\delta_T,\delta_R;t)$ was defined as

$$\rho^G_{kl,k'l,'n}(\delta_T,\delta_R;t) = \mathbb{E}\left[\frac{h^G_{kl,n}(t)[h^G_{k'l,'n}(t)]^*}{\left|h^G_{kl,n}(t)\right|\left|[h^G_{k'l,'n}(t)]^*\right|}\right] \quad (37)$$

where $[\cdot]^*$ denotes the conjugating operation.

2) The Normalized STFCF: The normalized STFCF was defined by

$$\begin{aligned}&\rho^G_{kl,k'l,'n}(\delta_T,\delta_R,\Delta f,\Delta t;t)\\ &= \mathbb{E}\left[\frac{[h^G_{kl,n}(t)]^* h^G_{k'l,'n}(t+\Delta t)e^{-j2\pi\Delta f\tau_n}}{\left|[h^G_{kl,n}(f,t)]^*\right|\left|h^G_{k'l,'n}(f+\Delta f,t+\Delta t)\right|}\right].\end{aligned} \quad (38)$$

3) The Time ACF: Let the antenna indexes be the same, $l = l,' k = k'$, and $\Delta f = 0$, the time ACF of the n-th cluster with the cluster evolution over the time axis, $\rho^G_{kl,n}(\Delta t;t)$ can be derived as

$$\begin{aligned}\rho^G_{kl,n}(\Delta t;t) &= \rho^G_{kl,k'l,'n}(0,0,0,\Delta t;t)\\ &= \mathbb{E}\left[\frac{[h^G_{kl,n}(t)]^* h^G_{kl,n}(t+\Delta t)}{\left|[h^G_{kl,n}(t)]^*\right|\left|h^G_{kl,n}(t+\Delta t)\right|}\right].\end{aligned} \quad (39)$$

4) The FCF: Also, let the antenna indexes be the same, $l = l,' k = k'$, and $\Delta t = 0$, the STFCF reduces to the FCF $\rho^G_{kl}(\Delta f;t)$

$$\begin{aligned}\rho^G_{kl}(\Delta f;t) &= \rho^G_{kl,k'l'}(0,0,\Delta f,0;t)\\ &= \mathbb{E}\left[\frac{\sum_{n=1}^{N_{\text{total}}}[h^G_{kl,n}(t)]^* h^G_{k'l,'n}(t)e^{-j2\pi\Delta f\tau_n}}{\left|[K^G_{kl}(f,t)]^*\right|\left|K^G_{k'l'}(f+\Delta f,t+\Delta t)\right|}\right]\\ &= \mathbb{E}\left[\frac{\sum_{n=1}^{N_{\text{total}}}\left|h^G_{kl,n}(t)\right|^2 e^{-j2\pi\Delta f\tau_n}}{\left|[K^G_{kl}(f,t)]^*\right|\left|K^G_{k'l'}(f+\Delta f,t+\Delta t)\right|}\right].\end{aligned} \quad (40)$$

5) The QSD: The non-stationarity and near-field effect have been observed as new properties for massive MIMO channels through channel measurements. The angular power spectrum (APS) varies significantly along the large array which was found in [49].

According to the above-mentioned channel model, the BS side is employed with M_T antenna elements and the number of MS side is M_R, respectively. For the BS, we select $M_T - L + 1$ groups over the Tx antenna array, and each group has L consecutive antennas. The group length L should be large enough for a clear vision of the spatial structure and to distinguish all AoDs for each antenna group. Thus, the correlation matrix for the BS side can be represented by

$$\mathbf{R}_T(i) = \mathrm{E}\left\{\mathbf{H}(i)^T\mathbf{H}(i)^*\right\}, \quad i = 1,\ldots,M_T - L + 1 \quad (41)$$

where i is the group index and equals to the index of its first antenna in the entire array. Here, $\mathbf{H}(i)$ is the $M_R \times L$ complex-valued channel matrix of the i-th antenna group which is time invariant. The correlation matrix distance (CMD) [50] between $\mathbf{R}_T(i)$ and $\mathbf{R}_T(j)$ is

$$d_{\text{corr}}(i,j) = 1 - \frac{\operatorname{tr}\{\mathbf{R}_T(i)\mathbf{R}_T(j)\}}{\|\mathbf{R}_T(i)\|_{\text{F}}\,\|\mathbf{R}_T(j)\|_{\text{F}}} \in [0,1]. \quad (42)$$

The QSD at the BS side is the maximum distance over which the CMDs remain below a certain threshold, denoted by

$$D^T_{qs}(i) = (\mu_{\max} - \mu_{\min} + L)\,\delta_T \quad (43)$$

where δ_T is the antenna element spacing. The minimum bound $\mu_{\min}$ of the QSD is defined by

$$\mu_{\min} = \underset{1\leqslant j\leqslant i-1}{\arg\max}\, d_{\text{corr}}(i,j) \geqslant c_{\text{th}} \quad (44)$$

and the maximum bound $\mu_{\max}$ of the QSD is defined by

$$\mu_{\max} = \underset{i+1\leqslant j\leqslant M_T-L+1}{\arg\min}\, d_{\text{corr}}(i,j) \geqslant c_{\text{th}} \quad (45)$$

where c_{th} denotes the CMD threshold. Within the QSD, the spatial structure is almost the same, i.e., the same set of clusters is seen by different antenna elements.

B. Statistical Properties of BDCM

The statistical properties of the proposed novel BDCM will attract more concentration, and we will discuss them in this section below.

1) Correlation Matrix: The correlation matrix of the novel BDCM can be expressed as

$$\begin{aligned}\mathbf{R}_{\mathbf{H}_B} &= \mathbb{E}\{\mathbf{H}_B(t)\mathbf{H}_B^H(t)\}\\ &= \mathbb{E}\{\mathbf{U}_R\widetilde{\mathbf{H}}_B(t)\mathbf{U}_T^H\mathbf{U}_T\widetilde{\mathbf{H}}_B^H(t)\mathbf{U}_R^H\}.\end{aligned} \quad (46)$$

Based on the previous expression of $\mathbf{U}_T$ and $\mathbf{U}_R$, we have

$$\begin{aligned}\mathbf{U}_T^H\mathbf{U}_T &= \sum_{m=1}^{M}\mathbf{e}_T^H(\theta_m)\,\mathbf{e}_T(\theta_m)\\ &= \sum_{m=1}^{M}\sum_{l=1}^{M_T}\mathbf{e}_T^*(l;\theta_m)\,\mathbf{e}_T(l;\theta_m) = M_T M\,\mathbf{I}\end{aligned} \quad (47)$$

where $\mathbf{I}$ is the unitary matrix. Similarly, we have $\mathbf{U}_R\mathbf{U}_R^H = 1/(M_R M)\,\mathbf{I}$. Thus, the correlation matrix can be derived as

$$\mathbf{R}_{\mathbf{H}_B} = M_T/M_R\,\mathbb{E}\{\widetilde{\mathbf{H}}_B(t)\widetilde{\mathbf{H}}_B^H(t)\} = M_T/M_R\,\mathbf{R}_{\widetilde{\mathbf{H}}_B}. \quad (48)$$

Therefore, the channel correlation matrix in the antenna domain is transformed into the beam domain. In this way, we can study the channel correlation from the beam domain and find some new characteristics.

2) The Space CCF: Similarly, the space CCF $\rho^B_{kl,k'l,'n}(\delta_T,\delta_R;t)$ of the novel BDCM can be calculated as

$$\rho^B_{kl,k'l,'n}(\delta_T,\delta_R;t)=\mathbb{E}\left[\frac{h^B_{kl,n}(t)[h^B_{k'l,'n}(t)]^*}{\left|h^B_{kl,n}(t)\right|\left|[h^B_{k'l,'n}(t)]^*\right|}\right]. \quad (49)$$

3) The Normalized STFCF: Like the GBSM, we express the time-varying transfer function $T^B_{kl}(f,t)$ as

$$T^B_{kl}(f,t)=\sum_{n=1}^{N_{\text{total}}}h^B_{kl,n}(t)e^{-j2\pi f\tau_n}. \quad (50)$$

The STFCF after the normalization $\rho^B_{kl,k'l'}(\delta_T,\delta_R,\Delta f,\Delta t;f,t)$ can be calculated as

$$\begin{aligned}&\rho^B_{kl,k'l'}(\delta_T,\delta_R,\Delta f,\Delta t;f,t)\\&=\mathbb{E}\left[\frac{[T^B_{kl}(f,t)]^*T^B_{k'l'}(f+\Delta f,t+\Delta t)}{\left|[T^B_{kl}(f,t)]^*\right|\left|T^B_{k'l'}(f+\Delta f,t+\Delta t)\right|}\right]\\&=\mathbb{E}\left[\frac{1}{\left|[T^B_{kl}(f,t)]^*\right|\left|T^B_{k'l'}(f+\Delta f,t+\Delta t)\right|}\right.\\&\left.\times\sum_{m=1}^{N_{\text{total}}}\sum_{n=1}^{N_{\text{total}}}[h^B_{kl,m}(t)]^*h^B_{k'l,'n}(t+\Delta t)e^{j2\pi[f\tau_m-(f+\Delta f)\tau_n]}\right].\end{aligned} \quad (51)$$

With the US assumption similar to the conventional GBSM, the STFCF in (51) reduces to

$$\begin{aligned}&\rho^B_{kl,k'l'}(\delta_T,\delta_R,\Delta f,\Delta t;t)\\&=\mathbb{E}\left[\frac{\sum_{n=1}^{N_{\text{total}}}[h^B_{kl,m}(t)]^*h^B_{k'l,'n}(t+\Delta t)e^{-j2\pi\Delta f\tau_n}}{\left|[T^B_{kl}(f,t)]^*\right|\left|T^B_{k'l'}(f+\Delta f,t+\Delta t)\right|}\right]\\&=\sum_{n=1}^{N_{\text{total}}}\mathbb{E}\left[\frac{[h^B_{kl,m}(t)]^*h^B_{k'l,'n}(t+\Delta t)e^{-j2\pi\Delta f\tau_n}}{\left|[T^B_{kl}(f,t)]^*\right|\left|T^B_{k'l'}(f+\Delta f,t+\Delta t)\right|}\right]\\&=\sum_{n=1}^{N_{\text{total}}}\eta_n\rho^B_{kl,k'l,'n}(\delta_T,\delta_R,\Delta f,\Delta t;t)\end{aligned} \quad (52)$$

where $\{\eta_n\}$ denotes the weight and we have $\sum_{n=1}^{N_{\text{total}}}\eta_n\rho^B_{kl,k'l,'n}(0,0,0,0;t)=1$. The normalized STFCF for the novel BDCM is defined by

$$\begin{aligned}&\rho^B_{kl,k'l,'n}(\delta_T,\delta_R,\Delta f,\Delta t;t)\\&=\mathbb{E}\left[\frac{[h^B_{kl,m}(t)]^*h^B_{k'l,'n}(t+\Delta t)e^{-j2\pi\Delta f\tau_n}}{\left|[h^B_{kl,m}(t)]^*\right|\left|h^B_{k'l,'n}(t+\Delta t)\right|}\right].\end{aligned} \quad (53)$$

4) The Time ACF: Let $p=p,'q=q'$, and $\Delta f=0$, $\rho^B_{kl,n}(\Delta t;t)$ can be derived as

$$\begin{aligned}\rho^B_{kl,n}(\Delta t;t)&=\rho^B_{kl,k'l,'n}(0,0,0,\Delta t;t)\\&=\mathbb{E}\left[\frac{[h^B_{kl,n}(t)]^*h^B_{kl,n}(t+\Delta t)}{\left|[h^B_{kl,n}(t)]^*\right|\left|h^B_{kl,n}(t+\Delta t)\right|}\right].\end{aligned} \quad (54)$$

5) The FCF: We set the antenna index to be the same, $p=p,'q=q'$, and $\Delta t=0$. The STFCF of BDCM in (53) will reduce to the FCF $\rho^B_{kl}(\Delta f;t)$

$$\begin{aligned}\rho^B_{kl}(\Delta f;t)&=\rho^B_{kl,k'l'}(0,0,\Delta f,0;t)\\&=\mathbb{E}\left[\frac{\sum_{n=1}^{N_{\text{total}}}[h^B_{kl,n}(t)]^*h^B_{k'l,'n}(t)e^{-j2\pi\Delta f\tau_n}}{\left|[T^B_{kl}(f,t)]^*\right|\left|T^B_{k'l'}(f+\Delta f,t+\Delta t)\right|}\right]\\&=\mathbb{E}\left[\frac{\sum_{n=1}^{N_{\text{total}}}\left|h^B_{kl,n}(t)\right|^2e^{-j2\pi\Delta f\tau_n}}{\left|[T^B_{kl}(f,t)]^*\right|\left|T^B_{k'l'}(f+\Delta f,t+\Delta t)\right|}\right].\end{aligned} \quad (55)$$

6) The QSD: The QSD analysis of the novel BDCM is similar with the GBSM, and we will not introduce here due to the limited space of the paper.

7) The Mean Square Error (MSE): As mentioned above, the sampling number of the arrival angles, also called as the beam number, is finite. The novel BDCM will be close to the GBSM when the number of beams become infinite. However, it is impossible to achieve infinite beam sampling in reality. The trade-off between the channel accuracy and beam number needs to be considered. The measured indicators can take advantage of the MSE between the statistical characteristics of the models.

Taking spatial correlation as an example, the formulas for calculating space CCFs of the two models have been given above. Let ρ^G_S and ρ^B_S represent the space CCFs of both models with the same antenna pairs and cluster at the same time instant.

$$\rho^G_S=\mathbb{E}\left[\frac{h^G_{kl,n}(t)[h^G_{k'l,'n}(t)]^*}{\left|h^G_{kl,n}(t)\right|\left|[h^G_{k'l,'n}(t)]^*\right|}\right] \quad (56)$$

$$\rho^B_S=\mathbb{E}\left[\frac{h^B_{kl,n}(t)[h^B_{k'l,'n}(t)]^*}{\left|h^B_{kl,n}(t)\right|\left|[h^B_{k'l,'n}(t)]^*\right|}\right]. \quad (57)$$

In this case, MSE ε of the spatial correlation is

$$\varepsilon=\mathbb{E}\left[\left||\rho^G_S-\rho^B_S\right||^2\right]. \quad (58)$$

V. System Property Analysis

A. Computational Complexity

Computational complexity is another important index of the channel model besides accuracy. In this paper, we use "real operations (ROs)" [47] to measure the computational complexity of the channel model. We have defined the amount of ROs for four basic real number operations, real multiplication, division, addition, and table lookup, as 1. Furthermore, other complex computations are combinations of these basic operations [48]. Table III defines the amount of ROs corresponding to several common mathematical operations.

1) The Conventional GBSMs: The computational complexity of the conventional GBSM is measured by the ROs of the channel impulse response (CIR) generation and the amount of ROs is calculated as

$$C_{\mathbf{H}^G}=C_{\mathbf{H}^{GL}}+C_{\mathbf{H}^{GN}}+1 \quad (59)$$

TABLE III
REQUIRED NUMBER OF ROS FOR TYPICAL MATHEMATICAL OPERATIONS

Operation	Required number of ROs
Exponential (e^x)	15
Uniform distributed random variable (RV)	5
Gaussian distributed RV	72
Complex multiplication	6
Complex division	11
Complex addition	2
Complex norm	5
$\sin(x)$	7
$\cos(x)$	8
$\tan(x)$	9
$\arcsin(x)$	7
$\arccos(x)$	8
$\arctan(x)$	9
Table lookup	1
$\log(x)$	1
Real square root	1

where $C_{\mathbf{H}^{\mathrm{GL}}}$ and $C_{\mathbf{H}^{\mathrm{GN}}}$ represent the amount of ROs for LOS and NLOS components of the GBSM, respectively. The amount of ROs for the LOS channel is

$$C_{\mathbf{H}^{\mathrm{GL}}} = 174 M_R M_T + 3. \tag{60}$$

The amount of ROs for the NLOS channel is

$$C_{\mathbf{H}^{\mathrm{GN}}} = N_{\text{total}}[(S-1)(208 M_R M_T + 19) + 4]. \tag{61}$$

According to (59), the amount of ROs for generating the conventional GBSM channel coefficients is

$$C_{\mathbf{H}^G} = 174 M_R M_T + 3 + N_{\text{total}}[(S-1)(208 M_R M_T + 19) + 4]. \tag{62}$$

2) The Novel BDCM: Similar to the conventional GBSM, the amount of ROs for generating the proposed BDCM can be calculated as

$$C_{\mathbf{H}^B} = C_{\mathbf{H}^{BL}} + C_{\mathbf{H}^{BN}} + 1 \tag{63}$$

where $C_{\mathbf{H}^{BL}}$ and $C_{\mathbf{H}^{BN}}$ represent the amount of ROs for LOS and NLOS components of the BDCM, respectively. The amount of ROs for the LOS channel is

$$C_{\mathbf{H}^{BL}} = 3 + [122(M_R + M_T) + 181]M. \tag{64}$$

The amount of ROs for the NLOS channel is

$$C_{\mathbf{H}^{BN}} = 3 + [122(M_R + M_T) + 77]M. \tag{65}$$

Therefore, according to (63), the amount of ROs for generating the novel BDCM channel coefficients is

$$C_{\mathbf{H}^B} = 6 + [244(M_R + M_T) + 258]M. \tag{66}$$

Let us take some typical parameter values as an example. When setting parameters as $M_T = 128, M_R = 32, N_{\text{total}} = 20, S = 20, M = 200$, we can calculate the computational complexities of both two models as

$$C_{\mathbf{H}^G} \approx 3.24 \times 10^8 \tag{67}$$

$$C_{\mathbf{H}^B} \approx 7.86 \times 10^6. \tag{68}$$

It can be seen that the computational complexity of novel BDCM is much lower than that of GBSM. Thus, the proposed BDCM can provide a simple model for further information theory and signal processing related researches.

B. Capacity Analysis

Generally, there are three levels to measure channel models, namely cluster level, link level and system level. Several statistical properties of channel models, such as space CCFs, time ACFs, and FCFs, are in the cluster level.

As one of the key indicators of communication system, channel capacity reflects link-level (single user), or even system-level (multi-user) performance for the channel models. For the validation of channel models, not only cluster-level analysis and validation are needed, but also from the perspective of the whole system, to measure the quality of a channel model, and channel capacity is a very good indicator. The average channel capacity with uniform Tx power allocation can be calculated as [51]

$$C = \mathbb{E}\left\{\log_2 \det\left(\mathbf{I} + \frac{\text{SNR}}{M_T}\bar{\mathbf{H}}\bar{\mathbf{H}}^H\right)\right\} \tag{69}$$

where $\det(\cdot)$ denotes the determinant operation, $\mathbf{I}$ is the $M_R \times M_T$ identity matrix, SNR denotes the signal-to-noise ratio and $\bar{\mathbf{H}}$ is the normalized channel matrix and can be obtained as

$$\bar{\mathbf{H}} = \mathbf{H} \cdot \left\{\frac{1}{M_T M_R}\sum_{k,l}|h_{k,l}|^2\right\}^{-\frac{1}{2}}. \tag{70}$$

C. SVS

The channel matrix can be expressed as singular value decomposition (SVD)

$$\mathbf{H} = \mathbf{U}\boldsymbol{\Sigma}\mathbf{V} \tag{71}$$

where $\mathbf{U}$ is an $M_R \times M_R$ unitary matrix, $\mathbf{V}$ is an $M_T \times M_T$ unitary matrix, and $\boldsymbol{\Sigma}$ is an $M_R \times M_T$ matrix. Furthermore, the SVS κ can be calculated as

$$\kappa = \frac{\max_i \sigma_i}{\min_i \sigma_i} \tag{72}$$

where σ_i $(i = 1, 2, \ldots, I)$ is the singular value of $\mathbf{H}$ and I is the smaller one of M_R and M_T.

VI. RESULTS AND DISCUSSIONS

The corresponding simulation model of the conventional GBSM is obtained by reducing (3) as

$$h^G_{kl,n}(t) = \delta(n-1)\sqrt{\frac{K}{K+1}}e^{j(2\pi f^{\mathrm{GL}}_{kl}t + \varphi^{\mathrm{GL}}_{kl})} + \sqrt{\frac{P_n}{K+1}}\frac{1}{\sqrt{S}}\sum_{i=1}^{S}e^{j(2\pi f_{n,i}t + \varphi_{kl,n,i})}. \tag{73}$$

Similarly, the corresponding simulation model of the novel BDCM is obtained by reducing (22) as

$$h^B_{kl,m}(t) = \sqrt{\frac{K}{K+1}}e^{j\left[2\pi f^{\mathrm{BL}}_{kl}t + \varphi_0 + \frac{2\pi}{\lambda}\left(D^R_{m_0,i} - D^T_{m_0,i}\right)\right]} \times e_R(k;\theta_{m_0}) \cdot e_T(l;\theta_{m_0})$$

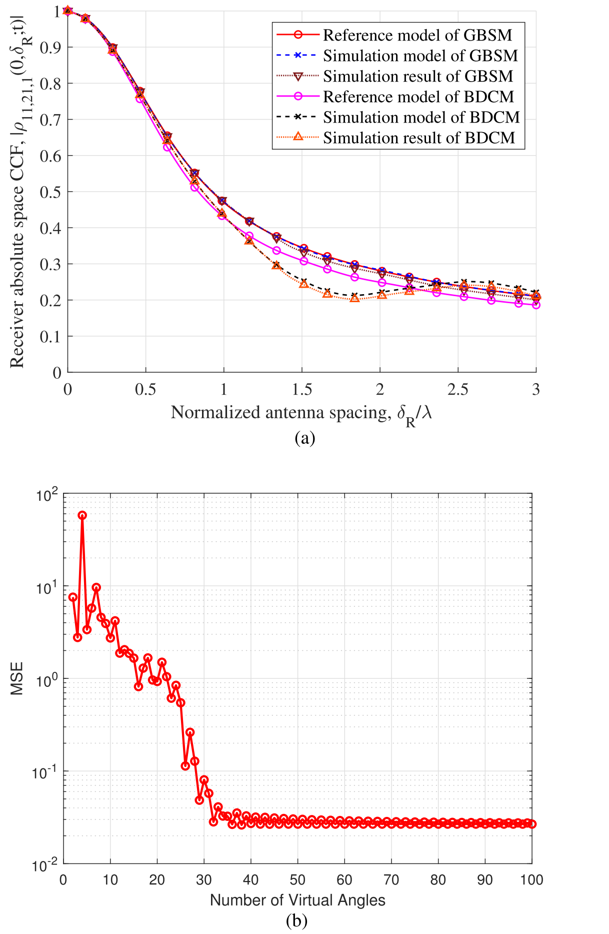

Fig. 4. (a) Absolute Rx space CCF $|\rho_{11,21,1}(0,\delta_R;t)|$ of both models and (b) MSE of simulation models ($M_R = 32$, $M_T = 32$, $t = 1$ s, $a_1 = 100$ m, $f = 80$ m, $D_c^a = 30$ m, $D_c^s = 50$ m, $\beta_R = \beta_T = \pi/2$, $\lambda = 0.12$ m, $f_{\max} = 33.33$ Hz, $\alpha_v = \pi/6$, $\kappa = 5$, $\bar{\alpha}_n^R = \pi/3$, NLOS). (a) Absolute Rx space CCF. (b) MSE of space CCF simulation models.

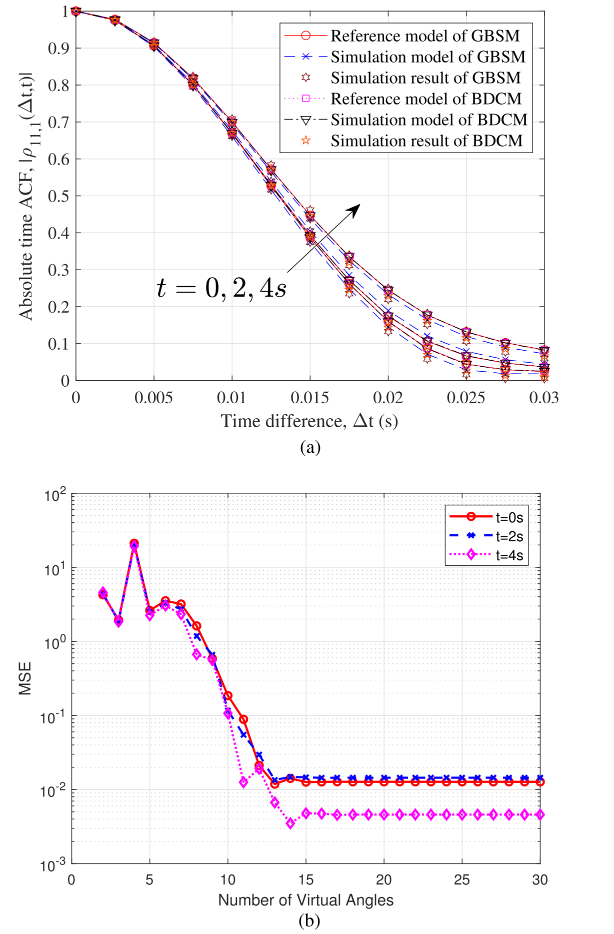

Fig. 5. (a) Absolute time ACF of Cluster$_1$ $|\rho_{11,1}(\Delta t;t)|$ for both models in comparison among t = 0, 2, 4 s and (b) MSE of simulation models ($M_R = 32$, $M_T = 32$, $a_1 = 100$ m, $f = 80$ m, $D_c^a = 15$ m, $D_c^s = 50$ m, $\beta_R = \beta_T = \pi/2$, $\lambda = 0.15$ m, $\delta_R = \delta_T = 0.5\lambda$, $f_{\max} = 33.33$ Hz, $v_c = 0.5$ m/s, NLOS, $\lambda_G = 80$ /m, $\lambda_R = 4$ /m, $P_F = 0.3$, $\kappa = 5$). (a) Absolute time ACF. (b) MSE of time ACF simuation models.

$$+\sqrt{\frac{P_m}{(K+1)M}}\sum_{m=1}^{M} e^{j\left[2\pi f_m t + \varphi_0 + \frac{2\pi}{\lambda}\left(D_{m,i}^R + D_{m,i}^T\right)\right]} \times e_R(k;\theta_m) \cdot e_T^*(l;\theta_m). \tag{74}$$

Fig. 4(a) compares the absolute values of space CCFs of two channel models. The reference model, simulation model and simulation result of each channel model are given in the figure. MSE of space CCF simulation models for both models are shown in Fig. 4(b). It can be observed that there is little difference between the reference models of both models, but only a small difference in the simulation models and the results. Therefore, we conclude that the gap between the novel BDCM and the conventional GBSM in space correlation is not large. In other words, the transformation of the channel model from the antenna domain to the beam domain does not greatly change the space correlation performance of the channel.

The correlation characteristics of two channel models in the time domain are compared in Fig. 5(a). The MSE of the time ACF simulation model of the two models is shown in Fig. 5(b), which changes with the time instant. As can be seen from the two figures, the novel BDCM also has the non-stationarity in the time domain, and there is little gap of the time correlation between both models. In other words, the transformation of the channel model from the antenna domain to the beam domain does not bring great performance loss to the time correlation performance of the channel.

The frequency correlation characteristics of the two models under different Rician K-factors are shown in Fig. 6. It can be observed that the frequency correlation characteristics of the two models are consistent at different frequency intervals and have similar frequency correlation performances. In addition, with the decrease of the Rician K-factor, the coherent frequency of the channel also decreases.

Fig. 7 shows an example plot of the estimated QSDs of both models for different Tx antenna group lengths. As we discussed above, the group length L should be large enough to observe the spatial structure and distinguish all the AoDs for each antenna group. It is observed that at the Tx antenna side, the QSDs of BDCM varies more dramatically than GBSM. The dramatic fluctuation is because the transformation of the channel model from the antenna domain to the beam domain, which makes the spatial non-stationarity of the model change dramatically.

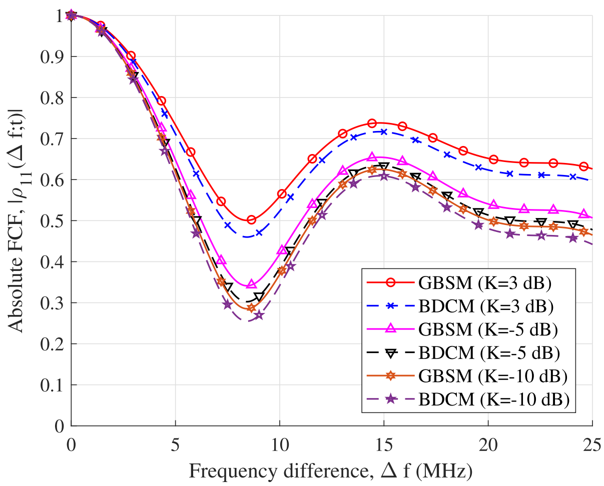

Fig. 6. Absolute FCF $|\rho_{11}(\Delta f;t)|$ comparison for both simulation models with different Rician factors K ($M_R = 32$, $M_T = 32$, $a_1 = 100$ m, $f = 80$ m, $D_c^a = 15$ m, $D_c^s = 50$ m, $\beta_R = \beta_T = \pi/2$, $\lambda = 0.15$ m, $\delta_R = \delta_T = 0.5\lambda$, $f_{\max} = 33.33$ Hz, $v_c = 0.5$ m/s, $\lambda_G = 80$ /m, $\lambda_R = 4$ /m, $\eta_c = 0.3$, $\kappa = 5$).

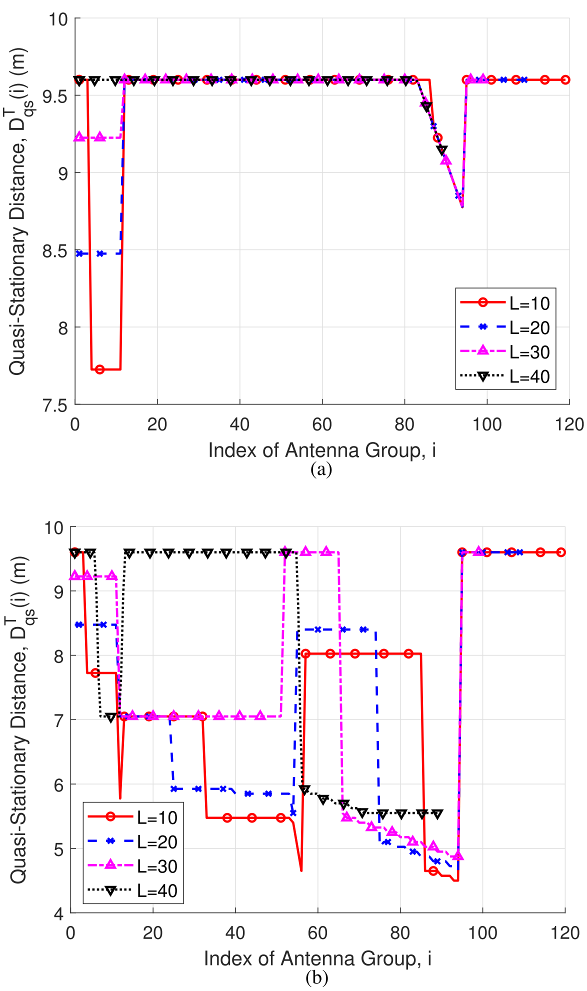

Fig. 7. Estimated quasi-stationarity distance of the conventional GBSM and novel BDCM for different Tx antenna group lengths ($M_R = M_T = 128$, $t = 1$ s, $a_1 = 100$ m, $f = 80$ m, $D_c^a = 30$ m, $D_c^s = 50$ m, $\beta_R = \beta_T = \pi/2$, $\lambda = 0.12$ m, $f_{\max} = 33.33$ Hz, $\alpha_v = \pi/6$, $\kappa = 5$, $\bar{\alpha}_n^R = \pi/3$, NLOS). (a) QSD of GBSM. (b) QSD of BDCM.

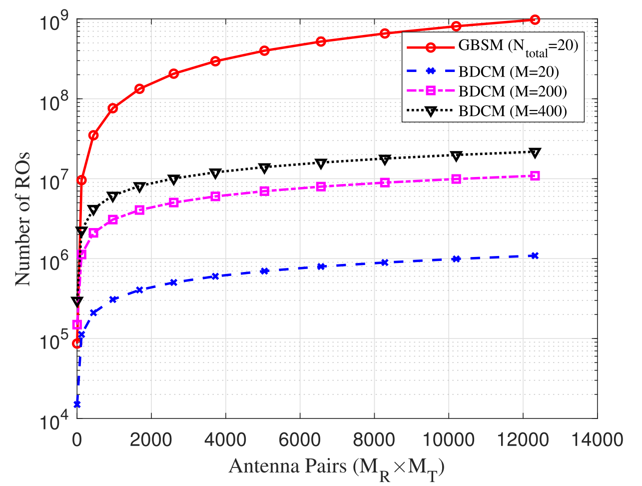

Fig. 8. Comparison of the computational complexity for both models ($M_R = M_T \in \{1, 10, \ldots, 120\}$, $N_{\text{total}} = 20$, $M \in \{20, 200, 400\}$).

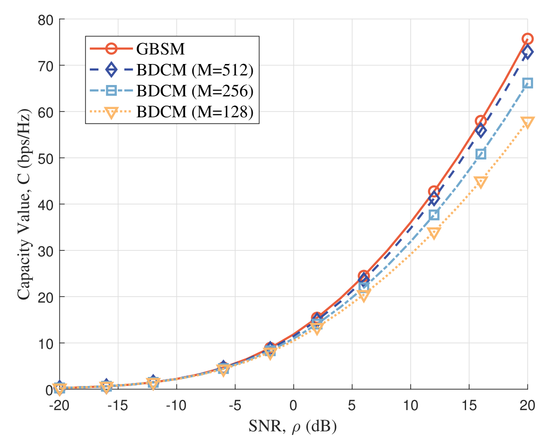

Fig. 9. Comparison of capacities between the simulation models of the GBSM and BDCM ($N_{\text{total}} = 30$, $M \in \{128, 256, 512\}$, $M_R = 128$, $M_T = 128$, $t = 1$ s, $a_1 = 100$ m, $f = 80$ m, $\beta_R = \beta_T = \pi/2$, $\lambda = 0.12$ m, $f_{\max} = 33.33$ Hz, $\alpha_v = \pi/6$, NLOS).

Since GBSM is modeled according to geometric relations, a scatterer distribution in a channel environment is assumed before modeling, and numbers of scatterers are randomly generated according to the distribution, as well as corresponding parameters such as power, delay and angle. In BDCM, virtual angles are introduced, that is, the space is divided into different angular (beam) sub-spaces, called beamspaces, with or without scatterers, and scatterers are generated randomly in these beamspaces. This means that the spatial non-stationarity of BDCM is more complex than that of GBSM. It needs to consider not only the non-stationarity between antennas, but also the non-stationarity between beams (that is, the scatterers observed by different beams are not exactly the same). Therefore, we can conclude that the domain transformation of the channel model will also affect the spatial non-stationarity.

In Fig. 8, we compare the computational complexity of two channel models with different numbers of antennas. Obviously, the computational complexity of the channel model increases

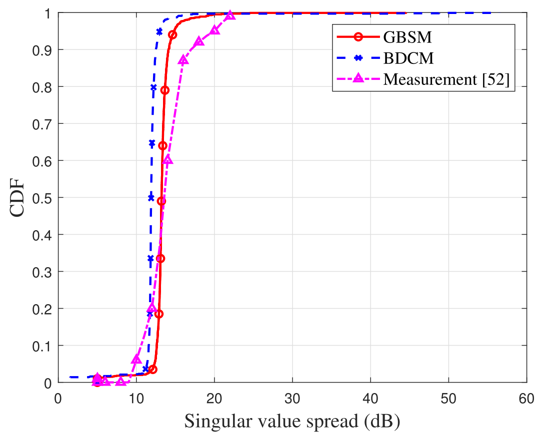

Fig. 10. CDFs of singular value spreads for both models and the measurement ($t = 1\,\mathrm{s}, a_1 = 100\,\mathrm{m}, f = 80\,\mathrm{m}, \beta_R = \beta_T = \pi/2, \lambda = 0.12\,\mathrm{m}, f_{\max} = 33.33\,\mathrm{Hz}, \alpha_v = \pi/6$, LOS).

with the increasing number of antennas. The smaller the sampling number of BDCM virtual angle, the lower the computational complexity is.

When simulating the channel capacities of the proposed BDCM, we selected several empirical values for beam numbers, which are multiplicatives of the antenna number, such as 128, 256, and 512. From simulation results shown in Fig. 9, it is found that the increase of the beam number will lead to the improvement of the accuracy for the BDCM. When the beam number reaches 512, the channel capacity of the proposed BDCM is very close to that of the GBSM.

The CDFs of SVSs of the BDCM, GBSM, and measurement are shown in Fig. 10. We observe that the SVSs of both models are close to those of the measurement [52], which demonstrates the accuracy of both channel models.

VII. Conclusion

A novel massive MIMO BDCM for B5G wireless communication systems considering the near-field effect and space-time non-stationarity has been proposed. For the first time, a GBSM has been transformed from the antenna domain to the beam domain, and a novel BDCM has been obtained. The space-time-frequency correlations, QSDs, computational complexities, channel capacities, and SVSs of both the GBSM and BDCM have been studied. Through the numerical and simulation results under the same conditions, we can conclude that the proposed novel BDCM has comparable performance as the GBSM but can significantly reduce the computational complexity. Also, both the novel BDCM and GBSM are close to the measurement. Thus, the proposed BDCM is more efficient for further information theory and signal processing related researches.

References

[1] X.-H. You et al., "Towards 6G wireless communication networks: Vision, enabling technologies, and new paradigm shifts," *Sci. China Inf. Sci.*, vol. 64, no. 1, Jan. 2021, Art. no. 110301, doi: 10.1007/s11432-020-2955-6.

[2] C.-X. Wang, J. Huang, H. Wang, X. Gao, X.-H. You, and Y. Hao, "6G wireless channel measurements and models: Trends and challenges," *IEEE Veh. Technol. Mag.*, vol. 15, no. 4, pp. 22–32, Dec. 2020.

[3] C.-X. Wang et al., "Cellular architecture and key technologies for 5G wireless communication networks," *IEEE Commun. Mag.*, vol. 52, no. 2, pp. 122–130, Feb. 2014.

[4] T. L. Marzetta, "Noncooperative cellular wireless with unlimited numbers of base station antennas," *IEEE Trans. Wireless Commun.*, vol. 9, no. 11, pp. 3590–3600, Nov. 2010.

[5] E. G. Larsson, O. Edfors, F. Tufvesson, and T. L. Marzetta, "Massive MIMO for next generation wireless systems," *IEEE Commun. Mag.*, vol. 52, no. 2, pp. 186–195, Feb. 2014.

[6] E. Björnson, E. G. Larsson, and T. L. Marzetta, "Massive MIMO: Ten myths and one critical question," *IEEE Commun. Mag.*, vol. 54, no. 2, pp. 114–123, Feb. 2016.

[7] C. F. López and C.-X. Wang, "A study of 2D non-stationary massive MIMO channels by transformation of delay and angular power spectral densities," *IEEE Trans. Veh. Technol.*, vol. 69, no. 12, pp. 14212–14224, Dec. 2020.

[8] X. Ge, B. Yang, J. Ye, G. Mao, C.-X. Wang, and T. Han, "Spatial spectrum and energy efficiency of random cellular networks," *IEEE Trans. Commun.*, vol. 63, no. 3, pp. 1019–1030, Mar. 2015.

[9] C.-X. Wang, J. Bian, J. Sun, W. S. Zhang, and M. Zhang, "A survey of 5G channel measurements and models," *IEEE Commun. Surv. Tut.*, vol. 20, no. 4, pp. 3142–3168, Oct.–Dec. 2018.

[10] S. Wu, C.-X. Wang, H. Haas, el-H. M. Aggoune, M. M. Alwakeel, and B. Ai, "A non-stationary wideband channel model for massive MIMO communication systems," *IEEE Trans. Wireless Commun.*, vol. 14, no. 3, pp. 1434–1446, Mar. 2015.

[11] X. Cai, G. Zhang, C. Zhang, W. Fan, J. Li, and G. F. Pedersen, "Dynamic channel modeling for indoor millimeter-wave propagation channels based on measurements," *IEEE Trans. Commun.*, vol. 68, no. 9, pp. 5878–5891, Sep. 2020.

[12] X. Cai, W. Fan, X. Yin, and G. F. Pedersen, "Trajectory-aided maximum-likelihood algorithm for channel parameter estimation in ultrawideband large-scale arrays," *IEEE Trans. Antennas Propag.*, vol. 68, no. 10, pp. 7131–7143, Oct. 2020.

[13] X. Cai and W. Fan, "A complexity-efficient high resolution propagation parameter estimation algorithm for ultra-wideband large-scale uniform circular array," *IEEE Trans. Commun.*, vol. 67, no. 8, pp. 5862–5874, Aug. 2019.

[14] H. Wu, S. Jin, and X. Gao, "Non-stationary multi-ring channel model for massive MIMO systems," in *Proc. Int. Conf. Wireless Commun. Signal Process.*, Nanjing, China, 2015, pp. 1–6.

[15] Y. Chen, Y. Li, S. Sun, X. Cheng, and X. Chen, "A twin-multi-ring channel model for massive MIMO system," in *Proc. 16th Int. Symp. Commun. Inf. Technol.*, Qingdao, China, 2016, pp. 606–610.

[16] S. Wu, C.-X. Wang, El-H. M. Aggoune, M. M. Alwakeel, and Y. He, "A non-stationary 3-D wideband twin-cluster model for 5G massive MIMO channels," *IEEE J. Sel. Areas Commun.*, vol. 32, no. 6, pp. 1207–1218, Jun. 2014.

[17] C. F. López and C.-X. Wang, "Novel 3-D non-stationary wideband models for massive MIMO channels," *IEEE Trans. Wireless Commun.*, vol. 17, no. 5, pp. 2893–2905, May 2018.

[18] A. O. Martinez, P. Eggers, and E. D. Carvalho, "Geometry-based stochastic channel models for 5G: Extending key features for massive MIMO," in *Proc. IEEE 27th Annu. Int. Symp. Pers. Indoor Mobile Radio Commun.*, Valencia, Spain, 2016, pp. 1–6.

[19] X. Gao, J. Flordelis, G. Dahman, F. Tufvesso, and O. Edfors, "Massive MIMO channel modeling - extension of the COST 2100 model," in *Proc. Joint NEWCOM/COST Workshop Wireless Commun.*, Barcelona, Spain, 2015, pp. 1–8.

[20] X. Gao, F. Tufvesson, and O. Edfors, "Massive MIMO channels - measurements and models," in *Proc. Asilomar Conf. Signals Syst. Comput.*, Pacific Grove, CA, USA, 2013, pp. 280–284.

[21] L. Liu et al., "The COST 2100 MIMO channel model," *IEEE Wireless Commun.*, vol. 19, no. 6, pp. 92–99, Dec. 2012.

[22] Y. Xie, B. Li, X. Zuo, M. Yang, and Z. Yan, "A 3D geometry-based stochastic model for 5G massive MIMO channels," in *Proc. 11th Int. Conf. Heterogeneous Netw. Qual. Rel. Secur. Robustness*, Taipei, Taiwan, 2015, pp. 216–222.

[23] S. Wu, C.-X. Wang, el-H. M. Aggoune, M. M. Alwakeel, and X. You, "A general 3-D non-stationary 5G wireless channel model," *IEEE Trans. Commun.*, vol. 66, no. 7, pp. 3065–3078, Jul. 2018.

[24] J. Bian, C.-X. Wang, X. Gao, X. You, and M. Zhang, "A general 3D non-stationary wireless channel model for 5G and beyond," *IEEE Trans. Wireless Commun.*, vol. 20, no. 5, pp. 3211–3224, May 2021.

[25] J. Bian, C.-X. Wang, Y. Liu, J. Tian, J. Qiao, and X. Zheng, "3D non-stationary wideband UAV-to-ground MIMO channel models based on aeronautic random mobility model," *IEEE Trans. Veh. Technol.*, vol. 70, no. 11, pp. 11154–11168, Nov. 2021.

[26] J. Wang et al., "A novel 3D non-stationary GBSM for 6G THz ultra massive MIMO wireless systems," *IEEE Trans. Veh. Technol.*, vol. 70, no. 12, pp. 12312–12324, Dec. 2021.

[27] C. F. Lopez, C.-X. Wang, and Y. Zheng, "A 3D non-stationary wideband massive MIMO channel model based on ray-level evolution," *IEEE Trans. Commun.*, vol. 70, no. 1, pp. 621–634, Jan. 2022.

[28] C.-X. Wang, Z. Lv, X. Gao, X.-H. You, Y. Hao, and H. Haas, "Pervasive channel modeling theory and applications to 6G GBSMs for all frequency bands and all scenarios," *IEEE Trans. Veh. Technol.*, vol. 71, no. 9, pp. 9159–9173, Sep. 2022.

[29] J. Huang, C.-X. Wang, H. Chang, J. Sun, and X. Gao, "Multi-frequency multi-scenario millimeter wave MIMO channel measurements and modeling for B5G wireless communication systems," *IEEE J. Sel. Areas Commun.*, vol. 38, no. 9, pp. 2010–2025, Sep. 2020.

[30] J. P. Kermoal, L. Schumacher, K. I. Pedersen, P. E. Mogensen, and F. Frederiksen, "A stochastic MIMO radio channel model with experimental validation," *IEEE J. Sel. Areas Commun.*, vol. 20, no. 6, pp. 1211–1226, Aug. 2002.

[31] W. Weichselberger, M. Herdin, H. özcelik, and E. Bonek, "A stochastic MIMO channel model with joint correlation of both link ends," *IEEE Trans. Wireless Commun.*, vol. 5, no. 1, pp. 90–100, Jan. 2006.

[32] A. M. Sayeed, "Deconstructing multiantenna fading channels," *IEEE Trans. Signal Process.*, vol. 50, no. 10, pp. 2563–2579, Oct. 2002.

[33] S. Noh, M. D. Zoltowski, Y. Sung, and D. J. Love, "Pilot beam pattern design for channel estimation in massive MIMO systems," *IEEE J. Sel. Topics Signal Process.*, vol. 8, no. 5, pp. 787–801, Oct. 2014.

[34] R. Couillet, M. Debbah, and J. W. Silverstein, "A deterministic equivalent for the analysis of correlated MIMO multiple access channels," *IEEE Trans. Inf. Theory*, vol. 59, no. 6, pp. 3493–3514, Jun. 2011.

[35] C. Wen, S. Jin, and K. Wong, "On the sum-rate of multiuser MIMO uplink channels with jointly-correlated rician fading," *IEEE Trans. Commun.*, vol. 59, no. 10, pp. 2883–2895, Oct. 2011.

[36] O. Huseyin, N. Czink, and E. Bonek, "What makes a good MIMO channel model?," in *Proc. IEEE 61st Veh. Technol. Conf.*, 2005, pp. 156–160.

[37] V. V. Veeravalli, Y. Liang, and A. M. Sayeed, "Correlated MIMO wireless channels: Capacity, optimal signaling, and asymptotics," *IEEE Inf. Theory*, vol. 51, no. 6, pp. 2058–2072, Jun. 2005.

[38] S. Dahiya, "A statistical block fading channel model for multiuser massive MIMO system," in *Proc. Int. Conf. Signal Process. Commun.*, Bengaluru, India, 2016, pp. 1–5.

[39] J. Joung, E. Kurniawan, and S. Sun, "Channel correlation modeling and its application to massive MIMO channel feedback reduction," *IEEE Trans. Veh. Technol.*, vol. 66, no. 5, pp. 3787–3797, May 2017.

[40] C. Sun, X. Gao, S. Jin, M. Matthaiou, Z. Ding, and C. Xiao, "Beam division multiple access transmission for massive MIMO communications," *IEEE Trans. Commun.*, vol. 63, no. 6, pp. 2170–2184, Jun. 2015.

[41] C. Sun, X. Gao, and Z. Ding, "BDMA in multicell massive MIMO communications: Power allocation algorithms," *IEEE Trans. Signal Process.*, vol. 65, no. 11, pp. 2962–2974, Jun. 2017.

[42] L. You, X. Gao, G. Y. Li, X.-G. Xia, and N. Ma, "BDMA for millimeter-wave/terahertz massive MIMO transmission with per-beam synchronization," *IEEE J. Sel. Areas Commun.*, vol. 35, no. 7, pp. 1550–1563, Jul. 2017.

[43] F. Zhu, F. Gao, H. Lin, S. Jin, J. Zhao, and G. Qian, "Robust beamforming for physical layer security in BDMA massive MIMO," *IEEE J. Sel. Areas Commun.*, vol. 36, no. 4, pp. 775–787, Apr. 2018.

[44] F. Lai, C.-X. Wang, J. Huang, X. Gao, and F.-C. Zheng, "A novel beam domain channel model for massive MIMO communication systems," in *Proc. IEEE Wireless Commun. Netw. Conf.*, Seoul, Korea, 2020, pp. 1–6.

[45] T. Zwick, C. Fischer, D. Didascalou, and W. Wiesbeck, "A stochastic spatial channel model based on wave-propagation modeling," *IEEE J. Sel. Areas Commun.*, vol. 18, no. 1, pp. 6–15, Jan. 2000.

[46] M. Patzöld, *Mobile Radio Channels*, 2nd ed., West Sussex, U.K.: Wiley, 2012.

[47] P. Kyosti and T. Jamsa, "Complexity comparison of MIMO channel modelling methods," in *Proc. 4th Int. Symp. Wireless Commun. Syst.*, Trondheim, Norway, 2007, pp. 1–5.

[48] Y. Zhang, A. Ghazal, C.-X. Wang, H. Zhou, W. Duan, and E. Maggoune, "Accuracy-complexity tradeoff analysis and complexity reduction methods for non-stationary IMT-A MIMO channel models," *IEEE Access*, vol. 7, no. 1, pp. 178047–178062, Dec. 2019.

[49] S. Payami and F. Tufvesson, "Channel measurements and analysis for very large array systems at 2.6GHz," in *Proc. 6th Eur. Conf. Antennas Propag.*, Prague, 2012, pp. 1–8.

[50] R. He et al., "Characterization of quasi-stationarity regions for vehicle-to-vehicle radio channels," *IEEE Trans. Antennas Propag.*, vol. 63, no. 5, pp. 2237–2251, May 2015.

[51] J. Zhang, Y. Zhang, Y. Yu, R. Xu, Q. Zheng, and P. Zhang, "3-D MIMO: How much does it meet our expectations observed from channel measurements?," *IEEE J. Sel. Areas Commun.*, vol. 35, no. 8, pp. 1887–1903, Aug. 2017.

[52] P. Harris et al., "Performance characterization of a real-time massive MIMO system with LOS mobile channels," *IEEE J. Sel. Areas Commun.*, vol. 35, no. 6, pp. 1244–1253, Jun. 2017.

Fan Lai (Student Member, IEEE) received the B.E. degree from Dalian Maritime University, Dalian, China, in 2015. He is currently working toward the Ph.D. degree in the National Mobile Communications Research Laboratory, Southeast University, Nanjing, China. His research interests include massive MIMO channel measurements and modeling and shortwave channel modeling.

Cheng-Xiang Wang (Fellow, IEEE) received the B.Sc. and M.Eng. degrees in communication and information systems from Shandong University, Jinan, China, in 1997 and 2000, respectively, and the Ph.D. degree in wireless communications from Aalborg University, Aalborg, Denmark, in 2004.

He was a Research Assistant with the Hamburg University of Technology, Hamburg, Germany, from 2000 to 2001, Visiting Researcher with Siemens AG Mobile Phones, Munich, Germany, in 2004, and Research Fellow with the University of Agder, Grimstad, Norway, from 2001 to 2005. Since 2005, he has been with Heriot-Watt University, Edinburgh, U.K., where he was promoted to a Professor in 2011. In 2018, he joined Southeast University, Nanjing, China, as a Professor. He is also a part-time Professor with Purple Mountain Laboratories, Nanjing, China. He has authored four books, three book chapters, and more than 480 papers in refereed journals and conference proceedings, including 27 highly cited papers. He has also delivered 24 invited keynote speeches/talks and 14 tutorials in international conferences. His research interests include wireless channel measurements and modeling, 6G wireless communication networks, and electromagnetic information theory.

Dr. Wang is the Member of the Academia Europaea (The Academy of Europe), European Academy of Sciences and Arts, the Fellow of the Royal Society of Edinburgh, IET, and China Institute of Communications, an IEEE Communications Society Distinguished Lecturer in 2019 and 2020, Highly-Cited Researcher recognized by Clarivate Analytics in 2017–2020, and one of the most cited Chinese Researchers recognized by Elsevier in 2021. He is currently an Executive Editorial Committee Member of the IEEE TRANSACTIONS ON WIRELESS COMMUNICATIONS. He was the Editor for more than ten international journals, including the IEEE TRANSACTIONS ON WIRELESS COMMUNICATIONS, from 2007 to 2009, IEEE TRANSACTIONS ON VEHICULAR TECHNOLOGY, from 2011 to 2017, and IEEE TRANSACTIONS ON COMMUNICATIONS, from 2015 to 2017. He was the Guest Editor of the IEEE JOURNAL ON SELECTED AREAS IN COMMUNICATIONS, Special Issue on Vehicular Communications and Networks (Lead Guest Editor), Special Issue on Spectrum and Energy Efficient Design of Wireless Communication Networks, and Special Issue on Airborne Communication Networks. He was also the Guest Editor of the IEEE TRANSACTIONS ON BIG DATA, *Special Issue on Wireless Big Data*, and IEEE TRANSACTIONS ON COGNITIVE COMMUNICATIONS AND NETWORKING, *Special Issue on Intelligent Resource Management for 5G* and Beyond. He was a TPC Member, TPC Chair, and General Chair for more than 80 international conferences. He was the recipient of 15 Best Paper Awards from IEEE GLOBECOM 2010, IEEE ICCT 2011, ITST 2012, IEEE VTC 2013Spring, IWCMC 2015, IWCMC 2016, IEEE/CIC ICCC 2016, WPMC 2016, WOCC 2019, IWCMC 2020, WCSP 2020, CSPS2021, WCSP 2021, IEEE/CIC ICCC 2022, 2020–2022 "AI 2000 Most Influential Scholar Award Honourable Mention" in recognition of his outstanding and vibrant contributions in the field of Internet of Things.

Jie Huang (Member, IEEE) received the B.E. degree in information engineering from Xidian University, Xi'an, China, in 2013 and the Ph.D. degree in communication and information systems from Shandong University, Jinan, China, in 2018.

From October 2018 to October 2020, he was a Postdoctoral Research Associate with the National Mobile Communications Research Laboratory, Southeast University, China, supported by the National Postdoctoral Program for Innovative Talents. From January 2019 to February 2020, he was a Postdoctoral Research Associate with Durham University, Durham, U.K. Since November 2020, he has been an Associate Professor with the National Mobile Communications Research Laboratory, Southeast University, China, and also a Researcher with Purple Mountain Laboratories, China. He is the Senior Member of China Institute of Communication. He has authored or coauthred more than 60 papers in refereed journals and conference proceedings. His research interests include millimeter wave, THz, massive MIMO, reconfigurable intelligent surface channel measurements and modeling, wireless Big Data, and 6G wireless communications. He was the recipient of the Best Paper awards from WPMC 2016, WCSP 2020, and WCSP 2021. He has also delivered seven Tutorials in IEEE/CIC ICCC 2021, IEEE PIMRC 2021, IEEE ICC 2022, IEEE VTC-Spring 2022, IEEE/CIC ICCC 2022, IEEE VTC-Fall 2022, and IEEE PIMRC 2022.

Xiqi Gao (Fellow, IEEE) received the Ph.D. degree in electrical engineering from Southeast University, Nanjing, China, in 1997.

In April 1992, he joined the Department of Radio Engineering, Southeast University. Since May 2001, he has been a Professor of information systems and communications. From September 1999 to August 2000, he was a Visiting Scholar with the Massachusetts Institute of Technology, Cambridge, MA, USA, and Boston University, Boston, MA, USA. From August 2007 to July 2008, he visited the Darmstadt University of Technology, Darmstadt, Germany, as a Humboldt Scholar. His research interests include broadband multicarrier communications, MIMO wireless communications, channel estimation and turbo equalization, and multirate signal processing for wireless communications. From 2007 to 2012, he was the Editor of the IEEE TRANSACTIONS ON WIRELESS COMMUNICATIONS, IEEE TRANSACTIONS ON SIGNAL PROCESSING from 2009 to 2013, and IEEE TRANSACTIONS ON COMMUNICATIONS from 2015 to 2017.

Dr. Gao was the recipient of Science and Technology awards of the State Education Ministry of China in 1998, 2006, and 2009, respectively, National Technological Invention Award of China in 2011, and the 2011 IEEE Communications Society Stephen O. Rice Prize Paper Award in the field of communication theory.

Fu-Chun Zheng (Senior Member, IEEE) received the B.Eng. and M.Eng. degrees in radio engineering from the Harbin Institute of Technology, China, in 1985 and 1988, respectively, and the Ph.D. degree in electrical engineering from the University of Edinburgh, Edinburgh, U.K., in 1992.

From 1992 to 1995, he was a Postdoctoral Research Associate with the University of Bradford, Bradford, U.K. Between May 1995 and August 2007, he was with Victoria University, Melbourne, VIC, Australia, first as a Lecturer and then as an Associate Professor in mobile communications. From September 2007 to July 2016, he was with the University of Reading, Reading, U.K., as a Professor (Chair) of Signal Processing. Since 2010, he has also been a Distinguished Adjunct Professor with Southeast University, China. Since August 2016, he has been with the Harbin Institute of Technology (Shenzhen), Shenzhen, China, as a Distinguished Professor. He was the recipient of the two U.K. EPSRC Visiting Fellowships - both hosted by the University of York (U.K.), first in August 2002 and then again in August 2006. For the past two decades, he has also carried out many Government and Industry sponsored Research Projects - in Australia, U.K., and China. His research interests include ultra-dense networks, ultra-reliable low latency communications, multiple antenna systems, green communications, and machine learning based communications.

He was the Editor (2001–2004) of IEEE TRANSACTIONS ON WIRELESS COMMUNICATIONS. In 2006, he was the General Chair of IEEE VTC 2006-S, Melbourne, Australia – the first ever VTC held in the southern hemisphere in VTC's history of six decades. He was the executive TPC Chair for IEEE VTC 2016-S, Nanjing, China – the first ever VTC held in mainland China. He was also the lead TPC Chair of IEEE VTC 2022-F (London and Beijing). He has been both a short term Visiting Fellow and a long term Visiting Research Fellow with British Telecom, U.K.